

# Self-sustaining smouldering combustion of coal tar for the remediation of contaminated sand



# Self-sustaining Smouldering Combustion of Coal Tar for the Remediation of Contaminated Sand: Two–Dimensional Experiments and Computational Simulations

**Tanzeer Hasan[12], Jason I Gerhard[1], Rory Hadden[13], and Guillermo Rein[4]**

[1] Department of Civil and Environmental Engineering, University of Western Ontario, London, Canada, jgerhard@uwo.ca

[2] Now at: Department of Geology, University of Dhaka, Dhaka, Bangladesh, thasan7@du.ac.bd

[3] Now at: Institute for Infrastructure and Environment, University of Edinburgh, Edinburgh, United Kingdom, r.hadden@ed.ac.uk

[4] Department of Mechanical Engineering, Imperial College London, London, United Kingdom, g.rein@imperial.ac.uk

Corresponding Author

*Jason I. Gerhard*
*Dept. of Civil and Environmental Engineering*
*The University of Western Ontario*
*Spencer Engineering Building, Rm. 3029*
*London, Ontario, Canada N6A 5B9*
*Phone: (519) 661-4154 Fax: (519) 661-3942*
*Email:* jgerhard@uwo.ca

POSTPRINT (ACCEPTED MANUSCRIPT)

Published:

*Hasan, T. JI Gerhard, R. Hadden, G. Rein. 2015. Self-sustaining smouldering combustion of coal tar for the remediation of contaminated sand: Two-Dimensional Experiments and Computational Simulations. Fuel, 150: 288-297.*

**Abstract**

This study presents the development and validation of a computational model which simulates the propagation of a smouldering front through a porous medium against unique experiments in coal tar and sand. The model couples a multiphase flow solver in porous media with a perimeter expansion module based on Huygens principle to predict the spread. A suite of two-dimensional experiments using coal tar-contaminated sand were conducted to explore the time-dependent vertical and lateral smouldering front propagation rates and final extent of remediation as a function of air injection rate. A thermal severity analysis revealed, for the first time, the temperature-time relationship indicative of coal tar combustion. The model, calibrated to the base case experiment, then correctly predicts the remaining experiments. This work provides further confidence in a model for predicting smouldering, which eventually is expected to be useful for designing soil remediation schemes for a novel technology based upon smouldering destruction of organic contaminants in soil.

*Keywords: smouldering, remediation, multiple dimensions, modelling, thermal severity*

## 1. Introduction

Fuels such as gasoline, diesel, crude oil and coal tar, are deposited in large amounts in the subsurface at tens to hundreds of thousands of sites due to poor historical disposal practices and ongoing accidental releases [1]. The presence of such Non-Aqueous Phase Liquids (NAPLs) in the subsurface pose human health and environmental hazards because of their toxicity and persistence. Despite the availability of several approaches, many NAPL remediation efforts fail to meet clean-up objectives with respect to the amount of contaminant removed, the time required, and/or the cost. Coal tar and heavy hydrocarbons remain among the most challenging to remediate: their long chain, complex, and multicomponent chemical structures resist transformation and breakdown by thermal, biological and chemical approaches [2]. When cleanup of these sites is required, excavation and disposal to a hazardous waste landfill or incinerator is typical, representing costly and unsustainable options.

STAR (Self-sustaining Treatment for Active Remediation) is a remediation technology that exploits the energy content of liquid organic contaminants, such as coal tar and heavy hydrocarbons, to achieve their *in situ* destruction by smouldering combustion. Smouldering is a flameless form of combustion, which propagates as an exothermic reaction wave driven by heterogeneous oxidation reactions (i.e., gas phase oxygen and condensed phase fuel) [3,4]. In general, smouldering combustion occurs within a solid porous medium which can be a permeable aggregate of particles, grains, or fibers where the fuel is either a combustible component of the porous matrix or a separate substance embedded in it [4]. The reaction can be self-sustaining in the presence of sufficient fuel, sufficient oxygen and limited heat losses [5,6].

Numerous porous solids can sustain a smouldering reaction, including polyurethane foam, coal, tobacco, dust, peat and wood [4]. The smouldering of polyurethane foam, in particular, has been extensively studied in the field of fire safety science (e.g. [7, 8, 9]). The majority of smouldering research has been conducted using one-dimensional (1D) experiments. These studies examined the effect of such parameters as air flux, buoyancy and moisture content on the propagation rate and temperature of the

smouldering reaction [6, 7, 10, 11]. In a 1D scenario, it is convenient to define the propagation direction of a smoulder reaction relative to the flow direction of the oxidizer. In forward smouldering, the reaction propagates in the same direction as the oxidizer flow, while in opposed smouldering the reaction propagates in the opposite direction [3, 4]. This has important implications for the heat and mass transfer during smouldering and consequently the reaction rate and temperature.

In many real systems, this simplification is no longer valid and smouldering propagation cannot be considered 1D. There are few multi-dimensional smouldering studies available in the literature but the process is expected to be influenced by many factors including ignition source geometry, fuel geometry and the influence of buoyancy [3]. Ohlemiller [3] summarized the available studies which included cellulose-based fuels (e.g., cardboard, shredded tobacco) examined under different fuel geometrics and with either buoyancy-induced air flows through the porous matrix or forced air flow across the free surface. These conditions were studied because they represent typical smouldering scenarios in a fire safety context. These studies revealed, for example, that the opposed smoulder velocity in cellulosic insulation was significant but weakly related to air flow rate applied across the top of the sample; meanwhile the velocity of the forward smouldering reaction on the surface was high and decreased with depth into the sample [12]. To the authors' knowledge, there are no publications on the spread of smouldering in two dimensions with a forced airflow applied through the porous medium instead of across the free surface.

Smouldering of organic liquids embedded in an inert porous medium has been studied in relatively few contexts. Fire flooding involves igniting a combustion reaction in deep wells to produce heat and gas waves for secondary oil recovery [13]. In contrast, STAR initiates smouldering to consume the organic liquids (NAPLs) and thereby remediate the sand [14]. The process is expected to be energy and cost efficient because, within the right parametric bounds, smouldering is self-sustaining; in other words, once initiated with a short, local energy input for ignition, the process requires no additional external energy to continue propagating. Switzer et al. [15] demonstrated STAR across a range of sands and NAPLs with

1D bench-top experiments. Pironi et al. [16] used column experiments to investigate the sensitivity of the STAR process to key parameters for coal tar and crude oil. Overall, those studies demonstrated that smouldering destruction is self-sustaining for a wide range of relatively non-volatile NAPLs in silts and sands when their concentrations in sands are above a minimum threshold (10,000 – 15,000 mg/kg at the bench scale). Even sands containing highly volatile NAPLs, which could not otherwise support a self-sustaining smouldering reaction, can be treated with STAR by injecting vegetable oil as a supplementary fuel [17]. These studies further demonstrated that, the sand through which the reaction passed exhibits non-detect concentrations of hydrocarbons, and the forward smouldering propagation rate linearly increased with the injected air flow rate. Switzer et al. [18] illustrated that STAR performed equally well when scaled up 1,000 times in a 3 $m^3$ test. Field pilot testing for in situ and ex situ applications of STAR are currently underway.

Numerical modelling is an important part of the process for designing and optimizing remediation systems. Numerical models of smouldering combustion are mainly 1D to reproduce the phenomenon observed in experimental forward or opposed propagation modes [5, 6, 8, 19-24]. However, two-dimensional (2D) models have been developed [25, 26] as well as one considering three dimensions [27]. These models aim to solve the heat and mass transfer processes that occur in a porous media as well as the chemical reactions and species generation and consumption. In all cases, simplifying assumptions are used to reduce the complexities associated with this multiphysics problem. Even with these simplifications, multi-physics numerical models of smouldering are computationally intense even for simulations at small (e.g., ~10 cm) scales [8]. As such, they are unsuitable for the field scale (~10 m to 100 m) domains required to explore smouldering as a site remediation technology.

MacPhee et al. [28] developed a novel, phenomenological approach to modelling smouldering with particular application to NAPLs in porous media. The ISSM (In Situ Smouldering Model) coupled a multiphase (air, NAPL) flow in porous media model and a geometric combustion front expansion model. This approach allows prediction of the movement of the propagating smouldering front as a function of

sand permeability, contaminant concentration, and air flux, with little computational demand. The low computational cost means that the model is suitable for application at the field scale even accounting for heterogeneous porous media. A disadvantage is that it requires calibration based on smouldering experiments for each fuel and sand type. The ISSM was calibrated against one-dimensional smouldering experiments for coal tar and crude oil in coarse sand [28]. Numerical testing of the ISSM verified that the model was robust under a variety of expected applications, numerically stable and computationally efficient [28]. MacPhee et al. [28] provided some demonstration 2D simulations, but acknowledged those results were speculative due to an absence of experimental data for validating 2D smouldering combustion predictions.

The main objective of this study was to compare the ISSM to 2D NAPL smouldering experiments and thereby increase confidence in its predictions of smouldering propagation in multidimensional scenarios. Eight experiments were conducted to evaluate the 2D smouldering behaviour of coal tar in sand for different air injection rates. A key difference between this study and previous smouldering research is the use of forced air injection that produces a multidimensional air flow field within the porous medium; this configuration was chosen as it is similar to how STAR is applied in the field. The experiments were quantified in terms of the vertical and lateral rate of smouldering front propagation as well as the overall extent of remediation. In addition, a thermal severity analysis was conducted to identify the critical temperature-residence time combinations that correspond to remediation of coal tar-contaminated sand. The ISSM was calibrated against one of the experiments for lateral combustion front propagation phenomena not previously observed. The calibrated model was then employed for independent simulations of the remaining experiments.

## 2. Methods

### 2.1 Experiments

Two-dimensional smouldering propagation experiments were carried out in a steel box 370 mm long × 300 mm high × 205 mm deep (Figure 1). NAPL-contaminated sand was prepared by mixing commercially available quartz sand (Number 12, Bell & MacKenzie Co., mean grain diameter = 0.88mm, coefficient of uniformity = 1.6) with commercial grade fresh coal tar (Alfa Aesar, density = 1180 kg/m$^3$ at 20°C). All of the experiments were conducted using a coal tar concentration of 71,000 mg/kg sand (NAPL saturation ~ 25%), which corresponds to typical field values and matches experiments previously conducted in 1D [16]. It is noted that, for smouldering studies, fresh coal tar is an appropriate surrogate for the weathered coal tar typically found at contaminated sites because both are dominated by high molecular weight compounds [29] that are involved in the exothermic (combustion) reactions occurring above 500°C [30].

In each experiment, the apparatus was packed in horizontal layers following established procedures [14, 15] modified to account for the geometry of the set-up. A 50 mm layer of clean sand was first packed into the apparatus, into which an air diffuser and heater were placed (Figure 1). Then 100mm of coal tar-contaminated sand was placed so as to ensure homogeneous packing. A further 50mm of clean sand was placed on top. This configuration has been shown to produce repeatable smouldering behaviour in 1D [14, 15].

The air diffuser was a set of perforated tubes connected to laboratory compressed air supply via a mass flow controller (FMA5400/5500 Series, Omega Ltd). The heater (450W, 120V, Watlow Ltd.) was coiled in a flat spiral with an outer diameter of 130 mm and covering an area of 0.325 cm$^2$ (equal to the area covered by the air diffuser). The heater was connected to a 120V AC, single-phase variable power supply (STACO Energy Products). The air diffuser and heater were asymmetrically located in the apparatus: 30 mm from the left wall and 210 mm from the right wall of the apparatus (Figure 1). Hereafter, the location

of the diffuser and heater will be referred to as the ignition source. The ignition source was located on the left side of the apparatus to (a) provide space for the reaction to propagate as far to the right as, while (b) ensuring that the right side boundary did not influence the air distribution, and while (c) keeping the apparatus to a size that would fit into our laboratory fume hood. Modelling and experiments indicate that the left wall had little influence on air velocities to the right of the diffuser and can be considered a no-flow boundary, while other simulations (discussed in Section 3.4.1) illustrate that the distance to the right side boundary was sufficient.

The contaminated sand was populated with 45 thermocouples (1.5mm x 500 mm, Type K, inconel-sheathed). Five thermocouples spaced at 20 mm vertical intervals were placed along the central axis of the heater to monitor upward vertical smouldering with the first thermocouple located 10mm from the bottom of the contaminated sand. The other 40 thermocouples were situated to monitor the lateral propagation of the smouldering front away from the ignition source; the first line of thermocouples was 10 mm from the right edge of the heater, and 25 mm separated each of the 8 lines, placing the last line 185 mm from the heater edge. The vertical locations of the five thermocouples in each line matched those along the heater centre line. The thermocouples were connected to a computer through a data logger (Multifunction Switch/Measure Unit 34980A, Agilent Technologies). The apparatus was wrapped in insulation (Roxul Comfort Batt R-15) to minimize heat losses thereby better simulating in situ conditions.

Following the procedure of [14, 15], smouldering was initiated by providing power to the heater until the contaminated sand 10 mm above the heater exhibited 500°C (approximately 100 min) and then initiating air injection at the predetermined rate. This ignited the smouldering reaction immediately, following which the heater was turned off (approximately 6 min after air injection was initiated). Air injection was continued, supporting self-sustaining smouldering, until the reaction naturally extinguished, defined by all thermocouples declining to ambient temperature.

The base case experiment, using an air injection rate of 350 L/min, was repeated three times to provide a measure of variability of the results (e.g., associated with packing, mixing, etc.). Five subsequent experiments employed air flow rates of 10, 50, 125, 250, and 450 L/min. This corresponds to a range of injected Darcy flux from 0.98 cm/s to 44.38 cm/s (volumetric flow rate injected divided by the cross-sectional area of the ignition source). The velocity of the smouldering front was calculated from the temperature-time data by an established procedure [14]. The final extent of front propagation (i.e., location of the boundary between the remediated and contaminated regions) was quantified by carefully excavating the apparatus in six 1.7 cm-thick lifts and, at each layer, photographing and measuring the position of the interface between the remediated and unremediated zones. The distinction between remediated and unremediated sand is very clear, since clean and dry sand exists wherever smouldering occurred; while the remediated zone was mapped by visual analysis in this work, previous studies with similar materials have quantified that post-STAR soils exhibit more than a 99.9% reduction in total petroleum hydrocarbons [15,16]

## 2.2 Modeling

The ISSM model formulation is described in full in [28]. The ISSM couples the multiphase flow model DNAPL3D with the Richards front expansion expressions to predict the spread of the smouldering front. DNAPL3D is a finite difference, two-phase flow numerical model that simulates the flows of a wetting and non-wetting phase in porous media by simultaneously solving their mass conservation equations [31, 32]. In this context, air is the nonwetting phase and coal tar is the wetting phase. The model incorporates capillary pressure-saturation-relative permeability relations validated against one [31, 32] and two-dimensional laboratory experiments [33]. In this application, the model predicts the evolution of air velocity vectors in 2D accounting for, amongst other things, the influence of local NAPL (fuel) content on local effective permeability to air.

The mathematical framework of the front expansion model, based upon Huygens principle, was developed by Richards [34, 35] for predicting the spread of wild land fires which, like smouldering, is controlled by local air velocity and fuel content [14, 15, 36]. Ignition is defined by a small ellipse at time t=0. Then, at the next time step after the air flow vectors are solved, new ellipses are generated at multiple locations on the perimeter of the initial ellipse and the new position of the smouldering front is the curve that passes through the vertices of all elliptical wavelets. Further details and the mathematical relationships for forward, opposed, and lateral propagation are presented in Supplementary Information.

It is acknowledged that in a two-dimensional scenario it is not accurate to speak of forward and opposed smouldering in the global sense as defined in traditional (1D) smouldering literature. However, it is possible to consider these at the local scale, where forward means in the direction of local air velocity vector, opposed is in the direction opposite to this vector, and lateral is in the direction perpendicular to this vector. Lateral front propagation is discussed in the fire spread literature where it refers to front advance in a direction perpendicular to the local air velocity vector. However, no acknowledgement of this phenomenon is found in the smouldering literature. Therefore, the consideration of lateral front propagation in the context of smouldering experiments and modelling appears to be unique to this study.

MacPhee et al. [28] calibrated the ISSM by minimizing the error between observed and predicted 1D forward smouldering velocities of coal tar in sand across a range of injection air flow rates (15 to 96 L/min) and contaminant concentrations (28,400 to 142,000 mg/kg). That work had to make assumptions about the opposed and lateral smouldering front velocity parameters, as well as the critical local minimum velocity leading to extinction, since 1D forward experiments provide no information about those processes. The validity of these assumptions, while not relevant to that study, are critical to this work as they directly impact predictions of 2D smouldering propagation and extinction along a lateral boundary. Further details on the parameter values assumed in that work and their re-evaluation in this work is provided in Section 3.4.

MacPhee et al. [28] demonstrated that the ISSM could be used to predict 2D smoulder front propagation in domains characterized by heterogeneous permeability and non-uniform contaminant concentration fields. In the absence of 2D experimental data, that work demonstrated that the predicted lateral extent of front spread in 2D simulations was highly sensitive to the lateral propagation rate parameter $\beta$ (in the range $\beta$ = 0 to 0.875). That study also predicted that the smouldering front would not penetrate low permeability media if the in situ air velocity was less than $\lambda$. However, that work could not make any conclusion about the actual magnitude of opposed smouldering velocity relevant for NAPLs (i.e., value of $\alpha$-$\kappa$), the rate or extent of lateral spread of smouldering (i.e., value of $\beta$), or the appropriate extinction criterion (i.e., value of $\lambda$) since none of these were tested in the 1D experiments.

The model domain was 0.37m × 0.20m in the horizontal and vertical directions, respectively, to represent a 2D slice (vertical cross section at the center) of the 2D box experiment. The domain was discretized into 11,840 nodes where each node was 0.0025m × 0.0025m. This discretization was demonstrated to balance front resolution and computational efficiency [28]. The sides and bottom boundaries were no flow to both DNAPL and air phases. The top boundary employed a fixed air pressure of 0.0 Pa (atmospheric). The air diffuser was defined by a linear, constant volumetric flux boundary. The initial shape of the front was defined as a small ellipse 0.13m along the major axisand 0.001m along the minor axis (i.e., circumscribing the ignition source). Clean and contaminated zones were defined identically to the experimental configuration.

The thermodynamic parameters, identical to those used by [28], are presented in Table S1, while the employed fluid and porous media properties are presented in Table S2 (Supplementary Information).

## 3. Results and Discussion

### 3.1 Base Case Experiment and Repeatability

Figure 2 presents the evolution of temperaturesat locations above the centre of the ignition source for the base case experiment (air injection rate of 350 L/min). This experiment was repeated three times with very similar results; throughout this section, all quantities will be presented as an average of the three repeats with an associated uncertainty that expresses the range of observed values across the three repeats. After the preheating period (see Figure 2 where 500°C was achieved at 10 mm (TC1) from the heater after 123min.), the air injection was started and the rapid rate of temperature increase indicated the initiation of smouldering [16]. The heater was turned off 6 min. later. A peak temperature of 1049 ± 88°C was observed at TC1 after 2.2 ± 0.2 min, after which the temperature there decreased since the NAPL (i.e., fuel) was consumed. Consequently, a characteristic succession of nearly equal temperature peaks at locations 50, 70, and 90 mm above the igniter (average = 908 ± 39°C) are observed, demonstrating a self-sustaining smouldering reaction [14, 15, 16]. The slightly elevated peak temperatures at TC1 and TC2 are a boundary effect commonly observed adjacent to an igniter and do not influence the self-sustainability of the reaction [16, 18]. Figure 2 reveals that approximately 9.0 ± 1.4 min. was required for the front to travel the vertical height of the contaminated sand layer. The calculated average upward smouldering front velocity was 1.04 ± 0.16 cm/min.

It is noted that similar experiments conducted in a column (with diameter approximately equal to that of the ignition source) observed a similar value for upward front velocity for approximately one-third of the volumetric air injection rate [16]. The difference is caused by the unidirectional air velocity vectors and 1D geometry that ensures all of the energy is transferred upwards (forwards) to the unburned fuel. It is noted that the peak temperatures in the base case were similar to those observed in the 1D experiments for coal tar in sand [16]. As expected, the same amount of energy is being generated per volume of coal tar oxidized. However, the local air velocities are lower here due to the multidimensional air distribution and

conduction and convection are spreading heat outwards from the ignition region. The influence of injected air flow rate on forward front velocity, as compared between 1D and 2D experiments, will be explored further in the modelling results.

The temperature profiles for the thermocouples situated to right of the igniter quantify the horizontal propagation of the smouldering front. They reveal that the front travelled simultaneously upwards and horizontally to the right from the ignition source. Figure 3 shows the peak temperature observed in the base case experiment as a function of height and horizontal distance from the ignition source. It reveals that horizontally along the base of the coal tar layer, peak temperatures never exceeded 400°C past 30 mm from the ignition source and thus smouldering never initiated here; this is because of limited air flow (and thus limited heat transfer from the smouldering zone) to this region. Meanwhile, along the top of the coal tar layer peak temperatures exceeded 400°C up to 90 mm to the right; this is consistent with convective heat transfer from the smouldering zone in a typical pattern where the reaction spreads outwards with height.

Photographs of the excavated experiment Figure S1, Supplementary Information) agree, demonstrating that the horizontal extent of the interface between the remediated and contaminated sand increases with height upwards from the ignition source. As with previous STAR studies [14, 15, 16, 18], samples in the remediated region were found to exhibit no detectable contamination and the contact line between remediated and unremediated sand was distinct. Figure 4 plots the horizontal location of the interface at each excavated height, with the range observed across the 3 repeats plotted as an error bar; the slight variation (±3.3 mm laterally) may be due to slight differences in packing of the contaminated sand and the duration of the preheating.

### 3.2 Thermal Severity

Thermal severity is expressed as a threshold temperature and residence time. Rein et al. [11] used this approach to quantify temperature-duration thresholds associated with smouldering wild fires and their impact on the soil. A thermal severity analysis has not been previously performed for STAR and the objective is to identify the critical temperature-residence time combinations that correspond to remediation of coal tar-contaminated sand under the conditions of the test. In each experiment, every thermocouple position was analyzed for the time experienced above a temperature threshold; the chosen thresholds corresponded to each 50°C increment between 200 and 800°C (i.e., 250, 300, 350°C, etc.). In Figure 5, each location is plotted at the highest temperature threshold it experienced, and the duration at that temperature. Each of the 130 data points plotted is identified as either remediated or not based on the post-test excavation results.

The figure reveals that coal tar remediation is associated with temperatures exceeding 550°C for more than 3.50 min., exceeding 600°C for more than 1.25 min, or exceeding 700°C for any duration. Note that a location was not remediated even if it experienced 500°C (but did not exceed 550°C) for more than 20 min. The coal tar destruction thermal severity criteria can therefore be defined as the blue line in Figure 5. For the purposes of data analysis in this work, the single criterion will be used: $T_{max}$>600°C for >1.25 min. The locations bounding the region where this criterion was exceeded/not exceeded in the base case experiment are plotted in Figure 4; they clearly match well the boundary between remediated and unremediated sand at the end of the experiment.

This suggests that this thermal severity criterion can be applied to the thermocouple data at any time in order to provide an estimate of the location of the remediation front as a proxy to the location of the smouldering front. For example, using this criterion, the experimentally determined evolution of the front for the base case experiment is presented for four times from ignition to extinction (coloured symbols in Figures 6a-d).

### 3.3 Sensitivity to Air Injection Rate

Experiments were conducted for air injection rates from 10 L/min to 450 L/min. The average upward front velocity along the centreline of the ignition source is shown to exhibit a linear relationship with injected air injection rates greater than 10L/min (Figure 7). A linear relationship is in agreement with 1D experiments [16] and is expected since smouldering is typically an oxygen-limited phenomenon [4, 5]. The lower threshold represents when the mass flux of oxygen is so low that the smouldering reaction does not generate enough energy to propagate. While relevant to this particular scenario, this represents the first time this threshold has been quantified for any forced air injection smouldering system.

Figure 8 plots the final position of the remediated/unremediated boundary for different air injection rates. For the 50 L/min experiment, the remediated region encompassed only the sand directly above the ignition source (i.e., essentially only upward propagation). As the air injection rate is increased, the horizontal spread is greater corresponding to the growing radius of influence of the air diffuser and the non-vertical spread of heat. Air injection rate is clearly not linearly related to outwards spread. Figure 8 reveals that the extent of horizontal remediation increases significantly with air injection rate from 50 to 250L/min, but only a small amount from 250 to 450 L/min. The lack of sensitivity observed at the higher air flow injection rates is likely because the radius of influence of the air flow has approached its upper limit in this apparatus due to the height of the free exit upper boundary; once the smouldering front reaches the upper clean layer, the dominant air flow trajectory is upwards through the remediated porous medium. It is expected that a taller apparatus with a thicker contaminated layer would allow differences in horizontal spreading to exist even at these higher air flowrates. In general, the pattern of smouldering front propagation and the degree of horizontal spread of the remediation zone reflects the evolving distribution of air velocity vectors.

The interface between the remediated and contaminated regions represents the extinction of the smouldering reaction. Extinction of smouldering reactions is associated with a shift in the energy balance, with increased heat loss relative to heat released and retained, beyond a critical threshold. Smouldering in the upwards direction benefits from buoyancy effects which aids he transport of the heat generated to preheat fuel ahead of the smoulder front, similar to 1D forward propagation [7]. In all of the cases examined with air flow larger than 10 L/min, complete remediation was observed directly above the ignition source because the forced oxidizer flow and buoyancy aligned resulting in a favourable, self-sustaining condition for heat and mass transfer ahead of the smouldering front. The spread of the smouldering front horizontally from the ignition source is controlled by two factors: (1) non-vertical air vectors that deliver oxygen and transport generated heat forwards along those non-vertical paths, and (2) lateral oxygen diffusion and heat conduction that propagate the reaction in a direction perpendicular to the (vertical or non-vertical) air velocity vectors. Both of these processes lead to smoulder propagation in a horizontal direction but also both are associated with heat losses at the reaction front to vertical buoyant flows. Therefore, the balance of energy, and thus the extinction threshold, shifts as a function of injected air flow rate up to a maximum as revealed in Figure 8. It is hypothesized in this work that the local extinction criterion approximately corresponds to a threshold magnitude of the local air velocity vector, which will be tested in the next section where these experiments are modelled.

### 3.4 Numerical Simulations

#### Model Calibration

First, the 1D-calibrated values used by MacPhee et al. [28] were applied to ISSM simulations of the 2D experiment (see Table 1). Figure 7 reveals that the model, using these values, is capable of capturing the observed average upwards smouldering velocity across the range of air injection rates that resulted in

smoulder propagation in the 2D apparatus. This means that the forward velocity equation (Equation S7) and its calibration parameter, *A*, apply equally from 1D to 2D scenarios.

Second, it was necessary to determine a relevant opposed propagation velocity (and thereby quantify ($\alpha - \kappa$) for the model). Opposed smouldering can be significant at modest air flow rates for smouldering solid fuels such as polyurethane foam [8]. However, across the entire range of experiments, including the lowest air injection rate of 50 L/min, no evidence of opposed smouldering was observed for coal tar-contaminated sand. Based on this result, it was determined that ($\alpha - \kappa$)= 0. Along with $\alpha + \kappa = 1$, this gives $\alpha$=0.5 and $\kappa$=0.5, which were assumed for all subsequent simulations in this work. With these values, the forward smouldering velocity exhibits the same dependence of local air velocity as the 1D-calibrated model (see Figure 7) and the opposed propagation rate is always zero for the air flow rates simulated in this work.

Third, the lateral propagation rate parameter $\beta$ was calibrated to the base case experiment by finding the minimum value of the error function: $\delta = \frac{\sum_{i=1}^{n} \left| X_E^i - X_S^i \right|}{n}$ where $\delta$ is the objective function value, $X_E^i$ is the experimental front position at a given time, $X_S^i$ is the simulated front position at the same time, and *n* is the number of data points (in this case, 6 corresponding to the 6 heights where the experimental front was measured). Simulations were carried out for values of $\beta$ in the range 0.050 to 0.450 and the function was evaluated at both 16 min and 20 minafter turning on air injection. These times were chosen because in this period the front was propagating laterally away from the ignition source, first quickly and then more slowly but not yet near extinction. Figure 9 reveals that $\beta$= 0.150 provided the best fit between the observed and simulated fronts at both times.

Fourth, a sensitivity study was conducted to evaluate the most appropriate extinction criterion. The most straightforward step was to calibrate $\lambda$. Recall that $\lambda$ is a local threshold value evaluated at every node along the front at every time step; the smouldering front will extinguish at any node where the magnitude of the air velocity is less than this threshold value. The boundary between the final remediated and contaminated regions in the base case experiment was simulated with a range of $\lambda$ values to find the minimum of the objective function above. Figure 9 reveals that $\lambda$= 0.056 m/s resulted in a predicted final front location that is most similar to that observed experimentally for the base case experiment.

The four step calibration procedure resulted in the set of parameters listed in Table 1. Figures 6a-d illustrate the base case scenario simulated with these parameters and compares the predicted position of the smouldering front to the front position estimated by the thermal severity criterion. Good agreement is observed at all times, including after 55.8 min, beyond which no movement is observed. This final extent of front spread compares well to that quantified by excavation (Figure 4).

Note that simulating the air flow pattern alone is insufficient for predicting the extent of remediation via smouldering. Contouring the air velocity field at intermediate times (figures not shown) reveals that the 0.056 m/s air velocity contour does not correspond to the final clean/contaminated boundary. Rather, it continually shifts to the left and only corresponds to the final clean/contaminated boundary at 55.8 min when it intersects with the propagating front moving to the right. The predicted air velocity field is influenced by the distribution of coal tar and, as the smouldering front propagates, there is feedback between them. The clean region, which exhibits a higher effective permeability to air than the contaminated region, continually grows and eventually intersects the top (free exit) boundary. Thus, an increasing fraction of the air bypasses the contaminated zone- which reduces air velocities in the contaminated region - over time. Thus, simulating both front propagation and airflow as tightly coupled processes is required to reproduce the observations.

### 3.4.1 Predictive Simulations

The calibrated model was used to simulate all of the other experiments to explore the validity of the calibration as a function of air injection rate. Figure 10 presents the positions of the simulated smouldering fronts at 2.5 min intervals from the start of air injection for all experiments besides the base case to allow comparison of the front propagation patterns and rates. Overall, it is observed that the experimental results are well predicted by the model across all air injection rates. The 10 L/min air injection rate is predicted to have zero front propagation, as observed, because nowhere along the initial front does the air velocity exceed the threshold value. For the rest of the cases in which self-sustaining propagation occurred, the simulated forward smouldering rates match those observed very well (see Figure 7). Simulations repeated in a domain twice as wide (figures not shown) demonstrated no change in the results shown in Figure 10, suggesting that the experimental box and numerical domain were wide enough to avoid any effect of the right side boundary on the outcomes.

Figure 11 compares the final predicted extent of remediation with that observed through excavation for all of the experiments; this is the most challenging evaluation since it represents late time behaviour at the smouldering extinction boundary. The agreement is acceptable, considering the heuristic nature of the model and the complex set of processes occurring in space and time. However, some discrepancies remain. The lack of smoothness of the simulated fronts is related to slight deviations in air velocity, with some nodes that are just above and others just below the threshold extinction value. In addition, the model predicts more sensitivity at the higher air injection rates than observed. This is likely because the extinction criterion used in the model (i.e., a minimum air velocity magnitude) is quite crude compared to the actual processes responsible for extinction (which include heat losses by convection and conduction, chemical kinetics as well as the local oxygen availability).

The results nevertheless suggest that the calibrated smoulder front spread model, combined with a simple extinction criterion, provides a useful tool to predict the extent of smouldering remediation and its

sensitivity to key simulated parameters such as air injection rate. It is worth commenting that the results shown in Figure 10, and the predictive abilities represented, are novel in the field of smouldering combustion. Moreover, each of those simulations took only about 20 mins on a desktop Intel duel core processor workstation. Field scale simulations with this model, predicting the spread of smouldering from a single ignition/air injection well at a contaminated site can be completed within one day. This represents a significant advance in the practical use of smouldering modelling for assisting engineering projects.

### 3.1 Summary and Conclusions

A set of experiments using coal tar-contaminated sand provided a unique data set for 2D smouldering propagation as a function of forced air injection rate. The radius of influence of the ignition source (i.e., the distance to the final boundary between remediated and contaminated sand) was found to increase with air injection rate. A thermal severity analysis revealed that coal tar-contaminated sand is expected to be locally remediated by smouldering if the maximum temperature observed is 700°C for any time, 600°C for more than 1.25 min., or 550°C for more than 3.5 min. While this result is likely specific to this contaminant/sand combination, the analysis technique is widely applicable and could provide thermal severity criteria for any smouldering system.

The upward smouldering velocities, linearly dependent on the injected air flow rate, were well predicted by a model calibrated to 1D experiments using similar materials. Two other model parameters were calibrated for the first time using this unique data set. The value of the local lateral propagation parameter indicates that the front spreads laterally at approximately 15% of rate that it spreads in the forward direction. This is the net result of heat conduction and oxygen diffusion and is a novel finding within smouldering research. A simple extinction criterion based upon a threshold magnitude of local air

flux was demonstrated to provide an acceptable prediction of the smouldering front extinction boundary given the heuristic nature of the model and the complexity of the phenomena considered.

The experiments illustrated that the radius of influence of the treated zone exhibited significant sensitivity to injected air flow rate before it intersected the upper free exit boundary but little sensitivity after; this may be representative of remediation within thin contaminated layers or within the vadose zone. However, in typical field scenarios, where remediation occurs well below the water table or in thick contaminated layers, the radius of influence of the treated zone is expected to increase with increased air flow rate over a much larger range and, ultimately, depend on the capacity of field equipment to deliver air and in situ conditions affecting the ultimate radius over which air is above the threshold minimum velocity for smouldering. Indeed, this has been observed in several field pilot tests of coal tar smouldering.

Simulations with this heuristic model are quickly completed relative to traditional smouldering numerical codes. Overall, the In Situ Smouldering Model was demonstrated to be a reliable engineering tool for simulating the propagation and extinction of 2D smouldering front movement in NAPL-contaminant sand across a wide range of air fluxes. The fact that the model was calibrated to a case where sensitivity to air flow rate was low, and yet the independent simulations successfully reproduce behaviour where sensitivity to the air flow rate is high, speaks to the strength of the model and this modelling process. This work provides evidence for the directional differences in liquid smouldering as well as building confidence in a tool that, with further development and validation at larger scales, is expected be useful for the designing STAR soil remediation schemes at the field scale.

It is acknowledged that the current calibration of the ISSM is specifically for coal tar in coarse sand. Although the model would need to be calibrated for each fuel/sand combination prior to application, the above framework represents a significant advancement of the state-of-the-art of smoulder modelling. Ongoing work is exploring the potential influence of simultaneous NAPL migration (due to reduced

viscosity at elevated temperature), verification of the model for heterogeneous domains, expansion to three-dimensional scenarios, and simulations of completed field pilot tests of in situ STAR remediation of coal tar. Considerations of the environmental implications of STAR are discussed in some depth in [17] and the field implementation (air delivery, extent of in situ remediation, management of emissions, etc.) will be explored in an upcoming publication on the field pilot tests.

## Acknowledgements

This research was supported by a grant to the second author from the Ontario Research Fund. We acknowledge the assistance of Tarek Rashwan with the laboratory experiments. Smouldering combustion of liquids as a remediation concept is patented under International PCT Filing PCT/GB2006/004591 and Granted Patents US 8,132,987 B2, CA 2,632,710, AU 2006323431 B9, JP4934832, and ZL 2006 8 0052554.X). The patent is owned by the University of Edinburgh and employed by the University of Western Ontario under a research license. Geosyntec Consultants, through its subsidiary Savron Smouldering Solutions, holds an exclusive license to commercialize the STAR technology.

## References

[1] Kueper, B.H., Stroo, H.F., Vogel., C.M., and Ward, C.H., 2014. Source zone remediation: The state of the practice. In: Chlorinated Solvent Source Zone Remediation, SERDP and ESTCP Remediation Technology Monograph Series, Eds. Kueper, Stroo, Vogel and Ward, Springer, New York. 713 pp.

[2] Hathaway, A.W., 2011. Remediation of Former Manufactured Gas Plants and Other Coal-Tar Sites. CRC Press, Boca Raton, FL. ISBN: 9780824791063, 1,398 pp.

[3] Ohlemiller, T. J., 2002. Smouldering combustion, SPFE Handbook of Fire Protection Engineering, 3rd ed., Massachusetts. In 200-210.

[4] Rein, G, 2014. Smouldering Combustion, Chapter 2-9 in: SFPE Handbook of Fire Protection Engineering, 5th Edition, Springer (in press).

[5] Ohlemiller, T. J., 1985. Modeling of smouldering combustion propagation. *Progress in Energy and Combustion Science*, 11 (4): 277-310.

[6] Torero, J. L. and Fernandez-Pello, A. C., 1996. Forward smoulder of polyurethane foam in a forced air flow. *Combustion and Flame,* 106 (1-2): 89-109.

[7] Torero, J. L. and Fernandez-Pello, A. C., 1995. Natural convection smoulder of polyurethane foam, upward propagation. *Fire Safety Journal,* 24 (1): 35-52.

[8] Rein, G.,Carlos Fernandez-Pello, A. and Urban, D. L., 2007. Computational model of forward and opposed smouldering combustion in microgravity. *Proceedings of the Combustion Institute,* 31 (2): 2677-2684.

[9] Ohlemiller, T. J. and Lucca, D. A., 1983. An experimental comparison of forward and reverse smoulder propagation in permeable fuel beds. *Combustion and Flame,* 54 (1-3): 131-147.

[10] Hadden, R., A Alkatib, G Rein, JL Torero, 2012. Radiant Ignition of Polyurethane Foam: the Effect of Sample Size, Fire Technology, doi:10.1007/s10694-012-0257-x.

[11] Rein, G.,Cleaver, N.,Ashton, C.,Pironi, P. and Torero, J. L., 2008. The severity of smouldering peat fires and damage to the forest soil. *CATENA,* 74 (3): 304-309.

[12] Ohlemiller, T. J., 1990. Forced smoulder propagation and the transition to flaming in cellulosic insulation. *Combustion and Flame,* 81 (34): 354-365.

[13] Akkutlu, I. Y. and Yortsos, Y. C., 2003. The dynamics of in-situ combustion fronts in porous media. *Combustion and Flame,* 134 (3): 229-247.

[14] Pironi, P.,Switzer, C.,Rein, G.,Fuentes, A.,Gerhard, J. I. and Torero, J. L., 2009. In *Small-scale forward smouldering experiments for remediation of coal tar in inert media*, Proceedings of the Combustion Institute, 1957-1964.

[15] Switzer, C.,Pironi, P.,Gerhard, J. I.,Rein, G. and Torero, J. R., 2009. Self-sustaining smouldering combustion: A novel remediation process for non-aqueous-phase liquids in porous media. *Environmental Science and Technology,* 43 (15): 5871-5877.

[16] Pironi, P.,Switzer, C.,Gerhard, J. I.,Rein, G. and Torero, J. L., 2011. Self-sustaining smouldering combustion for NAPL remediation: Laboratory evaluation of process sensitivity to key parameters. *Environmental Science and Technology,* 45 (7): 2980-2986.

[17] Salman, M., J.I. Gerhard, D. W. Major, P. Pironi, and R. Hadden, 2015. Remediation of trichloroethylene-contaminated soils by STAR technology using vegetable oil smoldering. Journal of Hazardous Materials, 285: 346 – 355.

[18] Switzer, C., Pironi, P., Gerhard, J.I., Rein, G., Torero, J.R., 2014. Volumetric scale-up of smouldering remediation of contaminated materials, Journal of Hazardous Materials, Volume 268, Pages 51-60, ISSN 0304-3894

[19] Dosanjh, S. S.,Pagni, P. J. and Fernandez-Pello, A. C., 1987. Forced cocurrent smouldering combustion. *Combustion and Flame,* 68 (2): 131-142.

[20] Schult, D. A.,Matkowsky, B. J.,Volpert, V. A. and Fernandez-Pello, A. C., 1995. Propagation and extinction of forced opposed flow smoulder waves. *Combustion and Flame,* 101 (4): 471-490.

[21] Schult, D. A.,Matkowsky, B. J.,Volpert, V. A. and Fernandez-Pello, A. C., 1996. Forced forward smoulder combustion. *Combustion and Flame,* 104 (1-2): 1-26.

[22] Buckmaster, J. and Lozinski, D., 1996. An elementary discussion of forward smouldering. *Combustion and Flame,* 104 (3): 300-310.

[23] Leach, S. V.,Rein, G.,Ellzey, J. L.,Ezekoye, O. A. and Torero, J. L., 2000. Kinetic and fuel property effects on forward smouldering combustion. *Combustion and Flame,* 120 (3): 346-358.

[24] Rein, G.,Lautenberger, C.,Fernandez-Pello, C.,Torero, J. and Urban, D., 2006. Application of Genetic Algorithms and Thermogravimetry to Determine the Kinetics of Polyurethane Foam in Smouldering Combustion. Elsevier.

[25] Moallemi, M. K.,Zhang, H. and Kumar, S., 1993. Numerical modeling of two-dimensional smouldering processes. *Combustion and Flame,* 95 (1-2): 170-182.

[26] Rostami, A.,Murthy, J. and Hajaligol, M., 2003. Modeling of a smouldering cigarette. *Journal of Analytical and Applied Pyrolysis,* 66 (1-2): 281-301.

[27] Saidi, M.,Hajaligol, M.,Mhaisekar, A. and Subbiah, M., 2007. A 3D modeling of static and forward smouldering combustion in a packed bed of materials. *Applied Mathematical Modelling*.

[28] MacPhee, S. L.,Gerhard, J. I. and Rein, G., 2012. A novel method for simulating smouldering propagation and its application to STAR (Self-sustaining Treatment for Active Remediation). *Environmental Modelling & Software,* 31: 84-98.

[29] Birak, P.S., and C.T. Miller, 2009. Dense non-aqueous phase liquids at former manufactured gas plants: challenges to modeling and remediation. Journal of Contaminant Hydrology, 105: 81-98.

[30] X. Sun, S. Yin, H. Wang, C. Li, and S. Zhang, 2012. Effect of the addition of cornstalk to coal powder/coal tar combustion. Journal of Thermal Analysis and Calorimetry, 109: 817-823.

[31] Gerhard, J. I. and Kueper, B. H., 2003a. Capillary pressure characteristics necessary for simulating DNAPL infiltration, redistribution, and immobilization in saturated porous media. *Water Resources Research,* 39 (8): SBH71-SBH717.

[32] Gerhard, J. I. and Kueper, B. H., 2003b. Relative permeability characteristics necessary for simulating DNAPL infiltration, redistribution, and immobilization in saturated porous media. *Water Resources Research,* 39 (8): 1213.

[33] Grant, G.P., Gerhard, J.I., and B.H. Kueper, 2007. Multidimensional validation of a numerical model for simulating a DNAPL release in heterogeneous porous media. *Journal of Contaminant Hydrology*, 92, pp. 109-128.

[34] Richards, G. D., 1990. An elliptical growth model of forest fire fronts and its numerical solution. *International Journal for Numerical Methods in Engineering,* 30 (6): 1163-1179.

[35] Richards, G. D., 1995. A General Mathematical Framework for Modeling Two-Dimensional Wildland Fire Spread. *International Journal of Wildland Fire,* 5 (2): 63-72.

[36] Finney, M. A., 1998. FARSITE: fire area simulator-model development and evaluation. USDA Forest Service Publication.

[37] Pironi, P., 2009. Smouldering combustion of liquids in porous media for remediating NAPL-contaminated soils. Ph.D Thesis, University of Edinburgh, Edinburgh, Scotland, UK.

[38] Green, D. W., Perry's Chemical Engineers' Handbook. 2008.

[39] Incropera, F. P. and DeWitt, D. P., Introduction to Heat Transfer. third ed ed.; John Wiley & Sons, New York.: 1996.

[40] Potter, M. C. and Wiggert, D., 2001. Mechanics of Fluids.

[41] Grant, G. P., 2005. The evolution of complex DNAPL releases: rates of migration and dissolution. *Ph.D. Thesis*, University of Edinburgh: Ediburgh, Scotland, UK, 429.

# TABLES

1

2 **Table 1: Smouldering Spread Model Values**

| Calibration Parameters | MacPhee et al. [28] | This Manuscript |
|---|---|---|
| Forward velocity calibration parameter, $A$ | 0.10 (fit to 1D data) | 0.10 (from [28]) |
| Local forward velocity constant, ($\alpha$+$\kappa$) | 1.0 (fit to 1D data) | 1.0 (from [28]) |
| Local opposed velocity constant, ($\alpha$-$\kappa$) | 0.750 (assumed) | 0.0 (fit) |
| Richard's constant, $\alpha$ | 0.875 (assumed) | 0.500 (fit) |
| Richard's constant, $\kappa$ | 0.125 (assumed) | 0.500 (fit) |
| Local lateral velocity constant, $\beta$ | 0 - 0.875 (varied) | 0.150 (fit) |
| Air magnitude threshold parameter, $\lambda$ | 0.5 m/s (assumed) | 0.056 m/s (fit) |

3

1

2 **FIGURES**

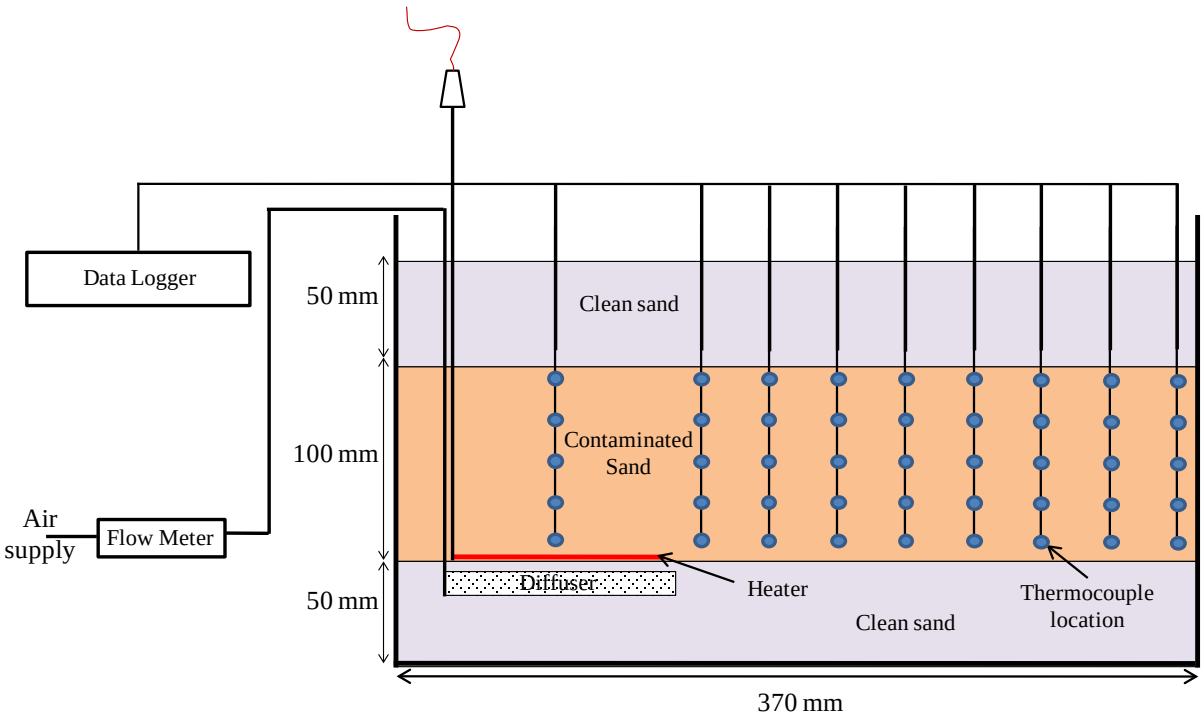


**Figure 1: Schematic of the experimental apparatus in cross-section and laboratory setup (not to scale).**

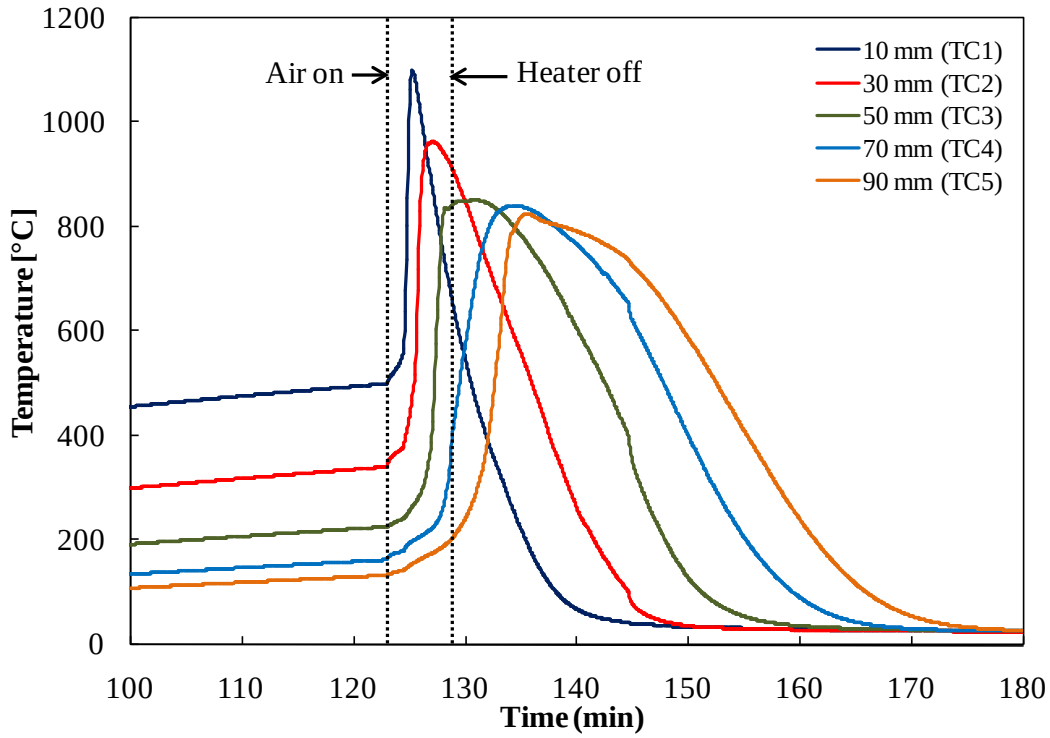


**Figure 2:Thermocouple profiles above the centre of the heater for base case experiment (air injection rate of 350 L/min). Profiles illustrate the propagation of a self-sustaining front vertically upwards from the ignition source. The legend indicates the distance of each thermocouple from the heater.**

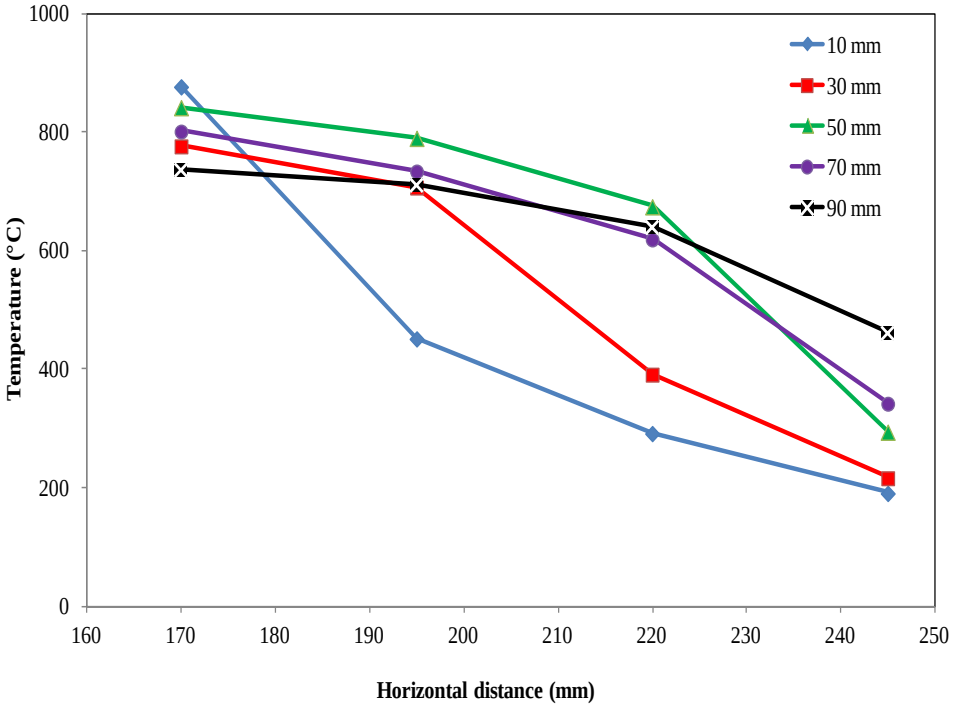


**Figure 3: Observed peak temperature as a function of horizontal distance for the base case experiment. The right edge of the heater is 160 mm from the left side of the domain. Each curve plots a single horizontal row of thermocouples identified by its height from the base of the contaminated sand.**

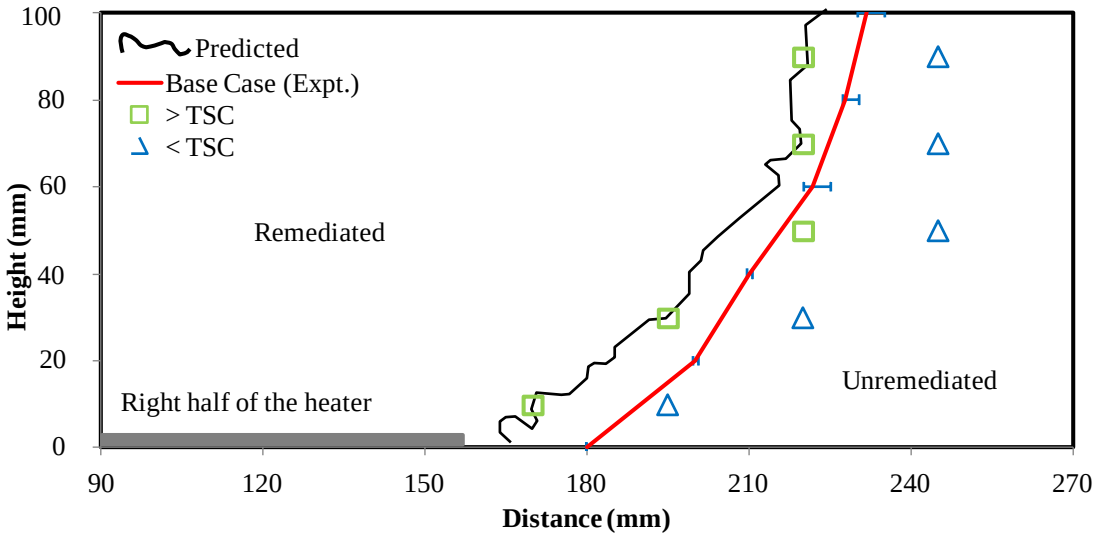


**Figure 4: Boundary between remediated and unremediated sand for the base case experiment, determined via excavation (red line, range of measurements across three repeats shown). The symbols represent thermocouple locations adjacent to the boundary that (i) exceeded the thermal severity criterion (TSC) (green squares), or (ii) never exceeded the TSC (blue triangles). The black line represents predicted final position of the front with the calibrated numerical model.**

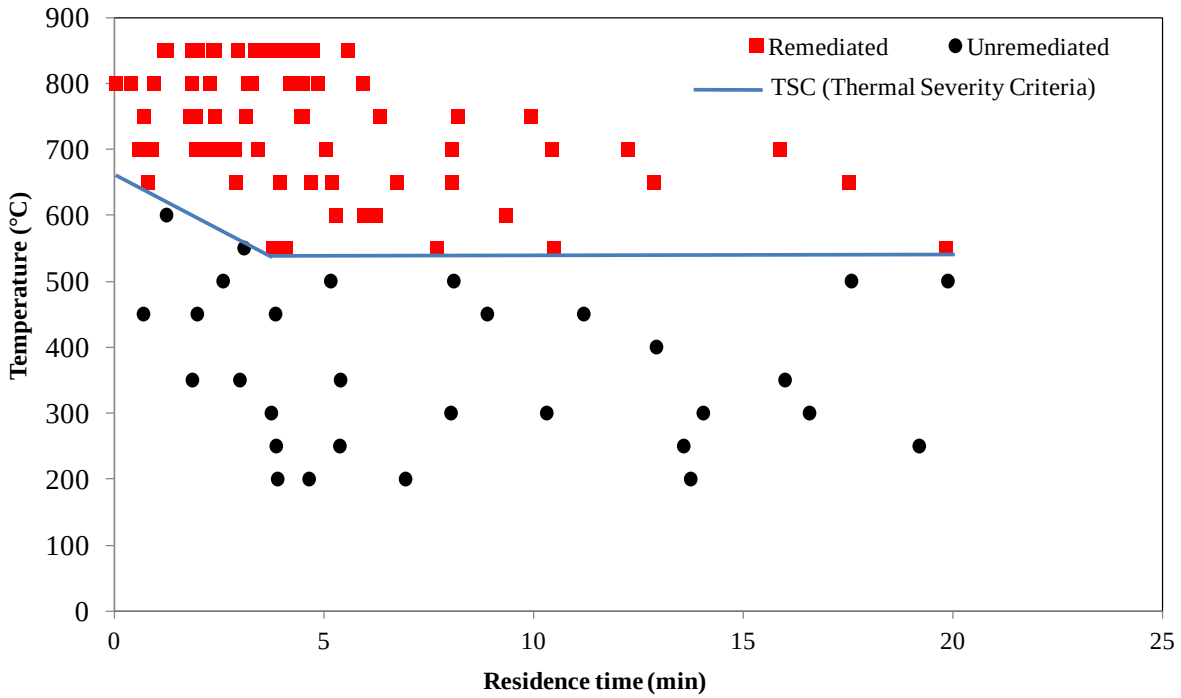


**Figure 5: Points represent the highest threshold temperature observed for each thermocouple across all experiments and whether that location was observed to be remediated. The line demarks the minimum residence time-threshold temperature combinations that correspond to remediation for coal tar in sand.**

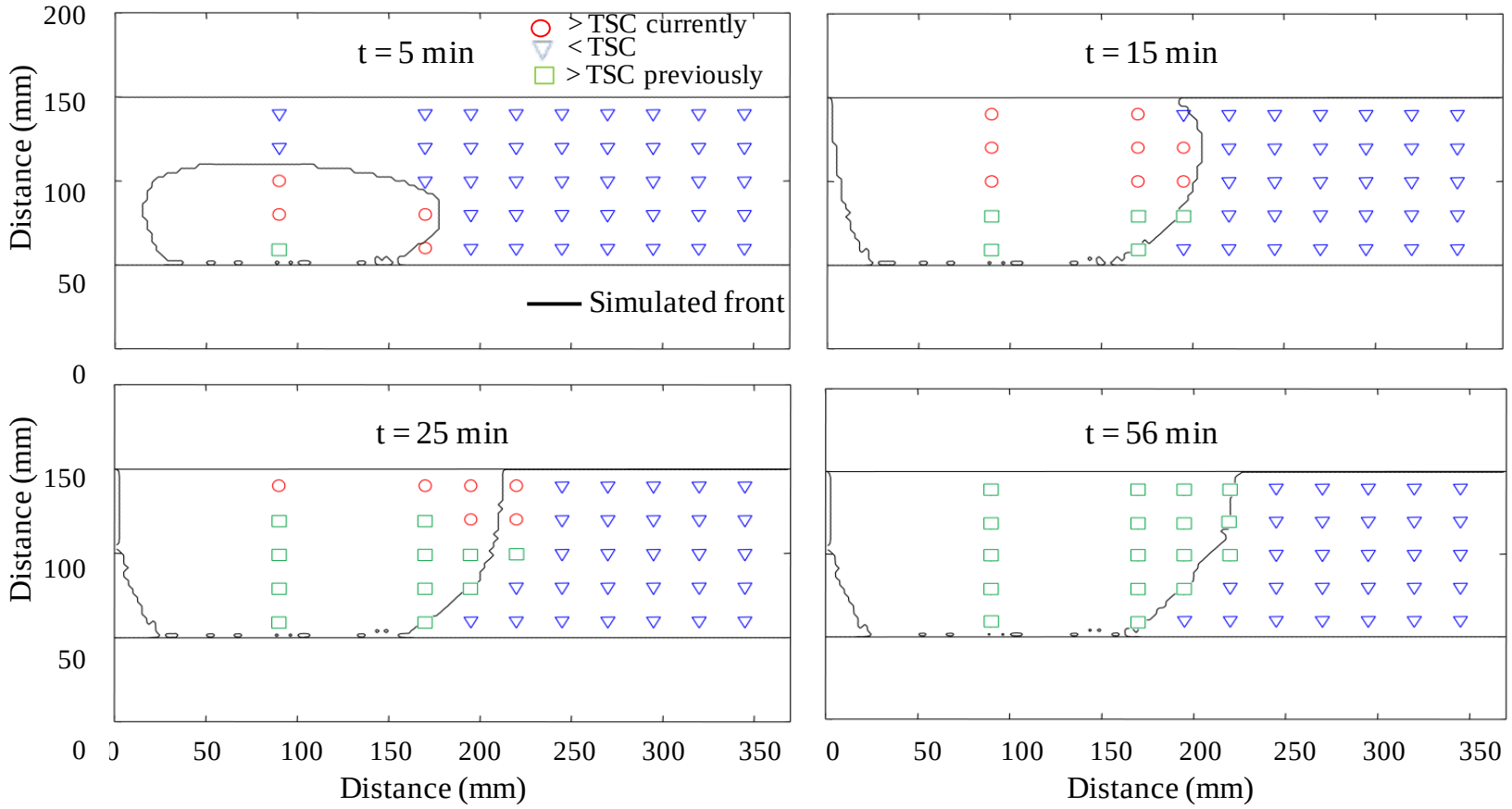


**Figure 6:Experimental results for the base case at four times plotting all thermocouple locations with respect to the thermal severity criterion (TSC): blue triangles = TSC not exceeded, red circles = TSC currently exceeded, green squares = TSC was exceeded but currently cooling. The black line plots the smouldering front position predicted by the numerical model.**

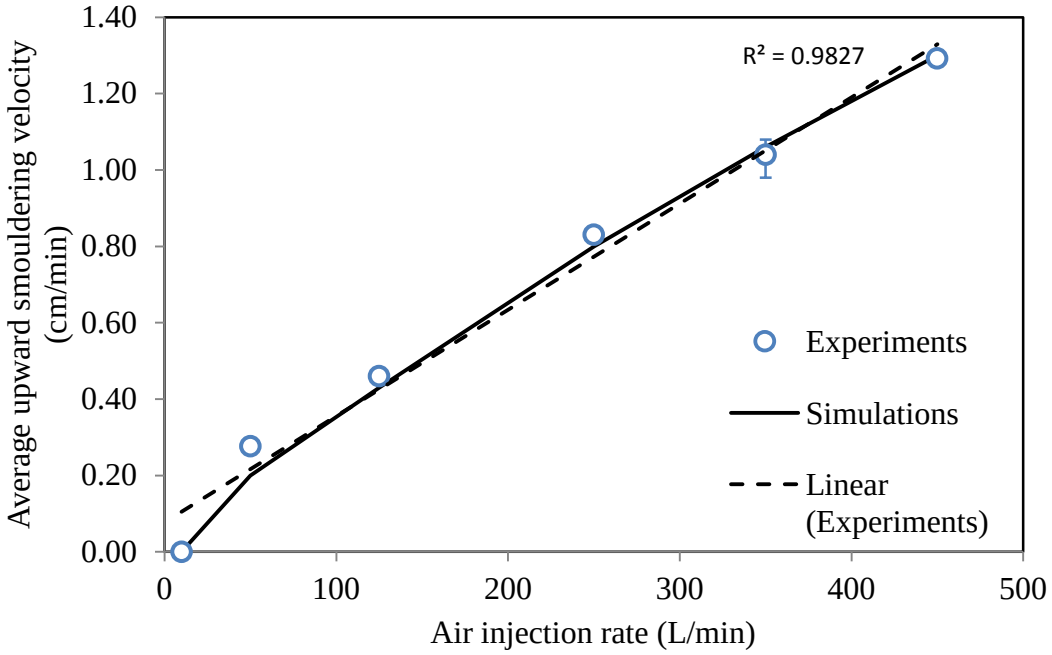


**Figure 7: Average upward smouldering velocity along the centreline of the ignition source versus air injection rate as observed in experiments and simulations. The error bar plots the range of velocities observed for three repeats of the base case. A best-fit linear regression of the experimental data is plotted for comparison purposes.**

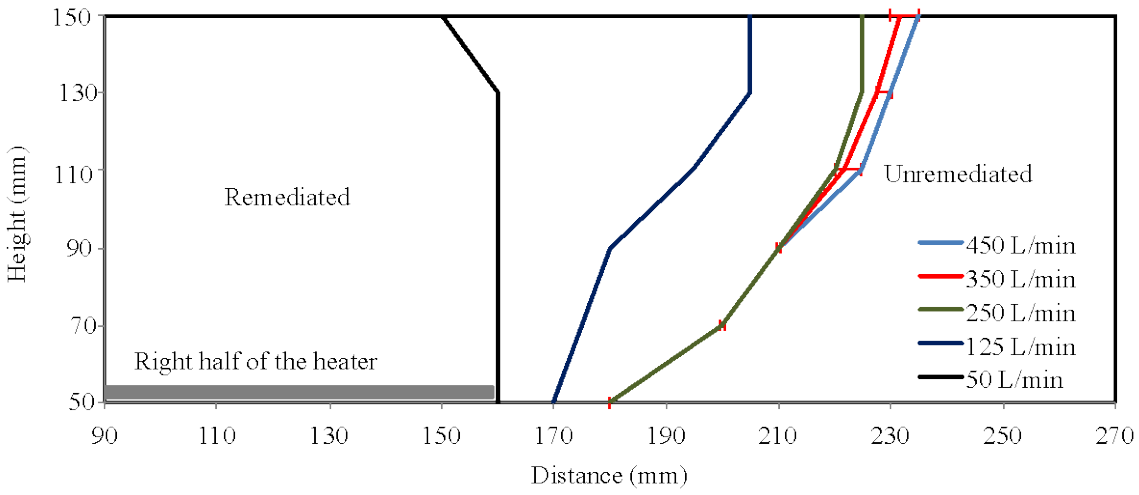


**Figure 8: The final extent of the remediated region versus air injection rates as measured during excavation. Note that some lines overlie each other. No remediation occurred for the 10 L/min experiment.**

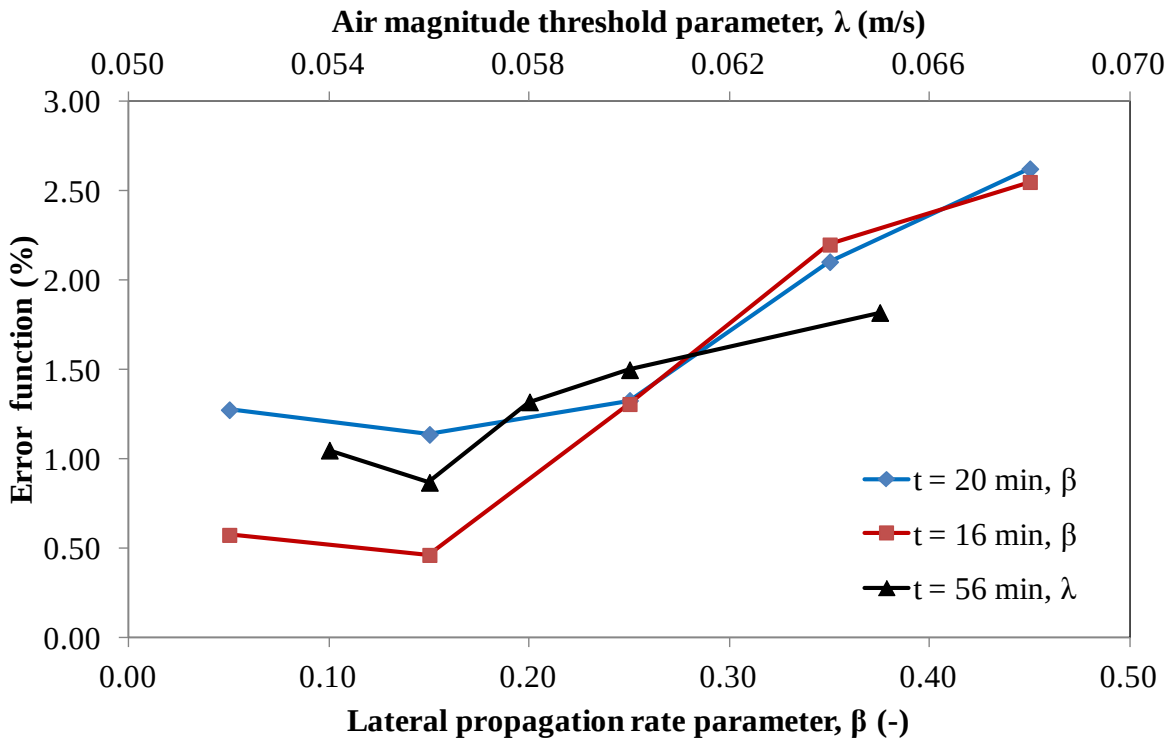


**Figure 9: Sensitivity of the fit between experimental and simulated smouldering front positions to (a) the lateral propagation rate parameter (*β* )at two intermediate times (when lateral spreading was significant), and (b) air magnitude threshold parameter (*λ*), evaluated at 56 min (when the actual front stopped moving). The lines connecting the data are only shown to aid in distinction of the data sets.**

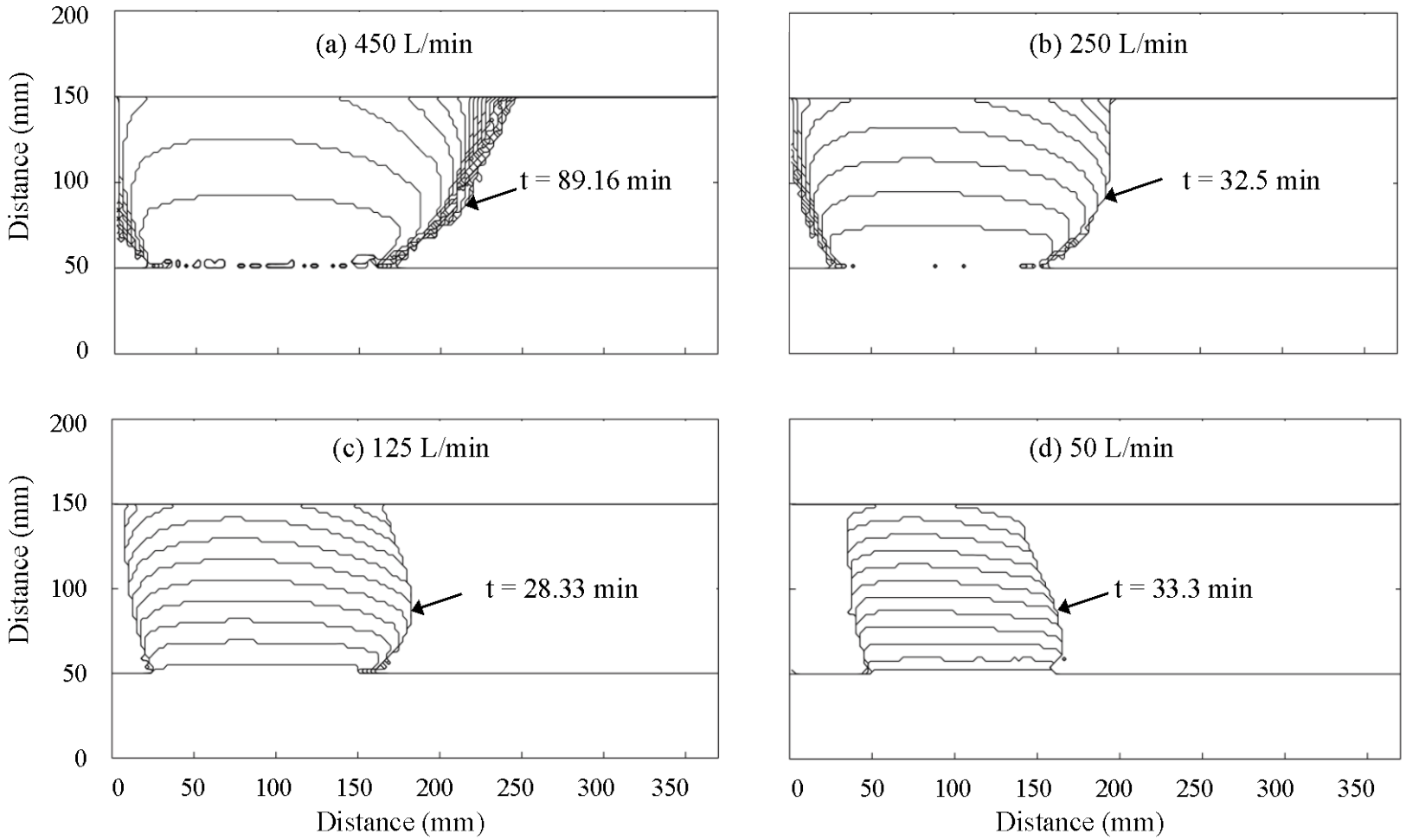


**Figure 10:Position of smouldering front predicted by the model at 2.5 min intervals for four air injection rates from the time air injection is initiated. Note that the predicted front is extinguished along the boundary, so this represents the final boundary between remediated and contaminated sand; the final time is shown in each case.**

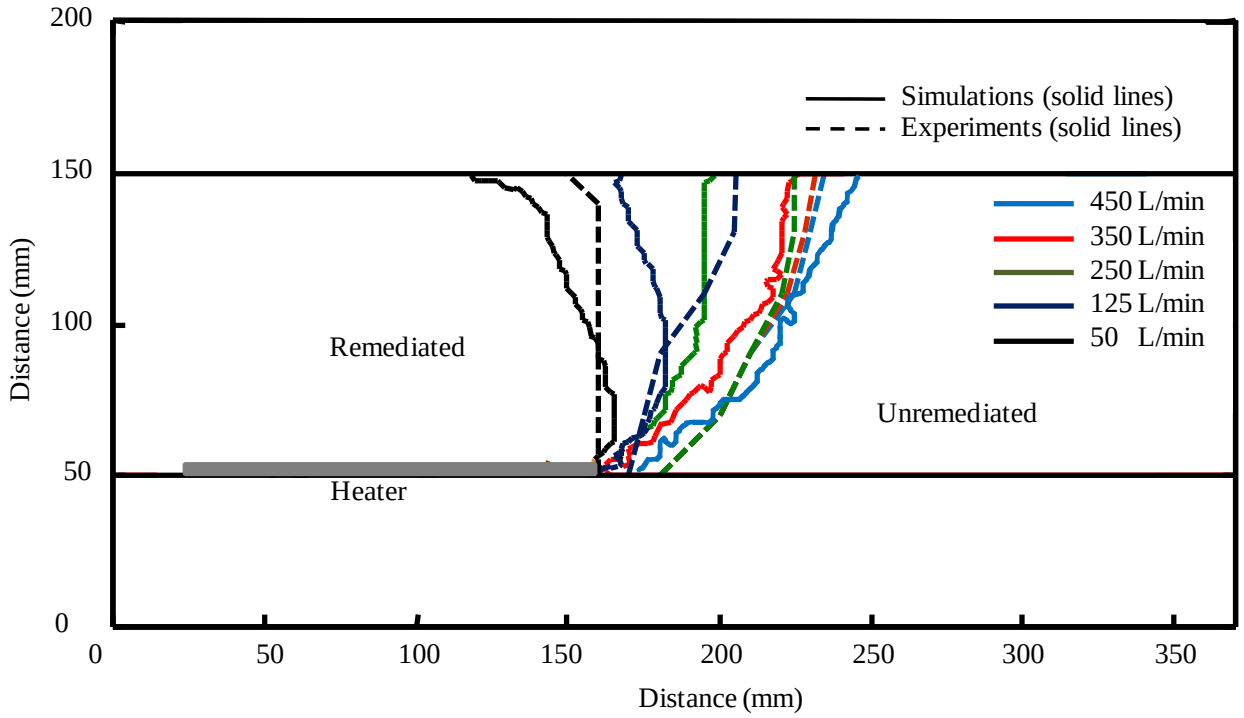


**Figure 11: Extent of remediation for five air injection rates observed in experiments (via excavation) and predicted by the calibrated model. No front propagation was predicted for the 10 L/min experiment, which matched the experiment.**

**SUPPLEMENTARY INFORMATION**

The mathematical framework of the front expansion model, based upon Huygens principle, was developed by Richards [34, 35]. Differential equations are used to represent the front parametrically where parameters *a* and *b* are half of the major and minor axes of the ellipse system, respectively, *c* is the rear focus of the ellipse, and $\theta$ is the angle that defines the local air flow direction [34, 35].

The variables *a*, *b* and *c*are defined locally and control the local shape and spread of the smouldering front [34, 35]:

$$V_{i,j}^{f}(t) = a_{i,j}(t) + c_{i,j}(t) \qquad i, j = x, y \tag{S1}$$

$$V_{i,j}^{l}(t) = b_{i,j}(t) \qquad i, j = x, y \tag{S2}$$

$$V_{i,j}^{o}(t) = a_{i,j}(t) - c_{i,j}(t) \qquad i, j = x, y \tag{S3}$$

where $V_{i,j}^{f}(t)$ , $V_{i,j}^{l}(t)$ and $V_{i,j}^{o}(t)$ are the local forward, lateral and opposed front propagation velocities, respectively, at a model node (*i, j*).

$a_{i,j}(t)$ , $b_{i,j}(t)$ and $c_{i,j}(t)$ can be linearly related with the forward smouldering rate [35]:

$$a_{i,j}(t) = \alpha V_{i,j}^{f}(t) \tag{S4}$$

$$b_{i,j}(t) = \beta V_{i,j}^{f}(t) \tag{S5}$$

$$c_{i,j}(t) = \kappa V_{i,j}^{f}(t) \tag{S6}$$

where, $\alpha$, $\beta$ and $\kappa$ are constants typically obtained from experiments. Considering Equations S1-S6, note that the value of ($\alpha$+$\kappa$) dictates the local forward velocity of smouldering, ($\alpha$-$\kappa$) dictates the local opposed velocity, and $\beta$ dictates the local lateral velocity. The local forward velocty is calculated at each node using an analytical expression based on global energy and mass conservation [6] adapted for a steady-state NAPL smouldering front [27]:

$$V_{i,j}^{f}(t) = \frac{m_{i,j}(t)C_g(T_s - T_g) + A\frac{\Delta H_r}{\nu_0} m_{i,j}(t) Y_{0,I}}{\left(\rho_{bs}C_s T_s - \left(\rho_{bs}C_s + S_{i,j}^{NAPL}(t)\varphi\rho_{NAPL}C_{NAPL}\right)T_{amb}\right)} \qquad i,j = x,y \qquad \textbf{(S7)}$$

Where $m_{i,j}$ represents the gas mass flux, $C_s$, $C_g$, and $C_{NAPL}$ are the specific heat constants for the solid, gas and NAPL phases, respectively, $T_S$ and $T_{amb}$ are the peak and ambient temperatures, respectively, $Y_{O,I}$ is the initial mass fraction of the oxygen present in the gas phase, $\varphi$ is the porosity, $S_{i,j}^{NAPL}$ represents the saturation of NAPL phase, $\rho_{bs}$ is the bulk density of the solid, $\Delta H_r$ is the effective heat of smouldering, $v_0$is the oxygen/fuel overall stoichiometric coefficient, and $A$ is a calibration parameter for a specific fuel type. A local extinction criterion was employed in which a local air velocity vector less than a critical magnitude, $\lambda$, would result in zero local smouldering velocity.

**Table S1: Thermodynamic Parameters for Simulations**

| **Parameters** | **Value** |
|---|---|
| Oxygen/fuel stoichiometric coefficient ($v_o$) | 2.89[a] |
| Effective heat of smouldering ($\Delta H_r$) | 39.4 (MJ/kg)[a] |
| Specific heat of the NAPL ($C_{NAPL}$) | 1880 ($J/kg_{NAPL}/K$)[b] |
| Smouldering temperature ($T_s$) | 1030 (K)[a] |
| Calibration parameter ($A$) | 0.10[f] |
| Initial mass fraction of oxygen in the gas phase ($Y_{0,I}$) | 0.235 ($kg_{O2}/kg_{gas}$)[b] |
| Specific heat of the gas ($C_q$) | 1100 (J/kg/K)[c] |
| Specific heat of the solid ($C_s$) | 1265 (J/kg/K)[b] |

[a][37]
[b][38]
[c][39]
[e] At temperature of 20°C.
[f] [27]

**Table S2: Modelling Fluid and Porous Media Properties**

| **Fluid and Soil properties** | **Value** |
|---|---|
| Surface tension ($\sigma$) | 0.033 (N/m)[a,b] |
| Density of air ($\rho_{air}$) | 1.204 ($kg/m^3$)[a,c] |
| Air viscosity ($\mu_{air}$) | 1.81 x $10^{-5}$ (Pa·s)[a,c] |
| NAPL density ($\rho_{NAPL}$) | 1180 ($kg/m^3$)[a,f] |
| NAPL viscosity ($\mu_{NAPL}$) | 7.59 (Pa·s)[a,d] |
| Mean particle diameter ($d$) | 1.5 (mm) |
| Intrinsic permeability ($k$) | 1.90 x $10^{-10}$ ($m^2$)[e] |
| Porosity ($\varphi$) | 0.38 |
| Displacement pressure ($P_D$) | 258.0 (Pa)[e] |
| Pore size distribution index ($\lambda$) | 3.41[e] |

[a] At temperature of 20°C.
[b] Pendent Drop Shape Method with an Axisymmetric Drop Shape Analyser.
[c][40]
[d] Brookfield DV III Rheometer.
[e][41]
[f]Pycnometer Method (ASTM Standard).

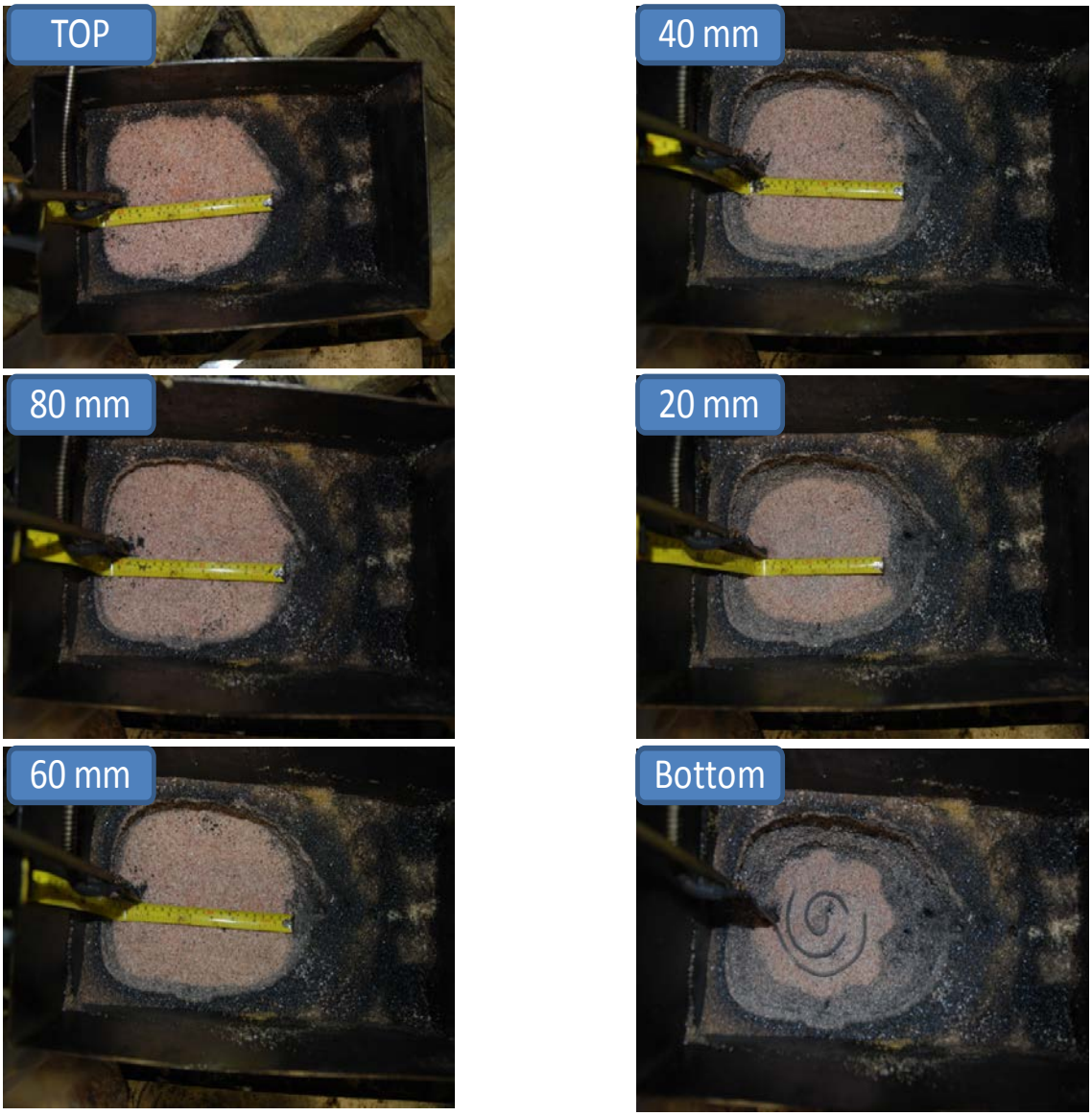


**Figure S1: Post-test excavation of the base case experiment. Intermediate elevations are labelled with their distance from the heater at the bottom. Horizontal spreading was measured at the center of the box as shown with the measuring tape.**